Three-Dimensional Structure of the Immunophilin-like Domain of FKBP59 in Solution[†,‡]

Constantin T. Craescu,[*,§] Nathalie Rouvière,[§,||] Aurel Popescu,[⊥] Esther Cerpolini,[§] Marie-Claire Lebeau,[||] Etienne-Emile Baulieu,[||] and Joël Mispelter[§]

Institut National de la Santé et de la Recherche Médicale U350, Institut Curie, Orsay 91405, France, Department of Biophysics, University of Bucarest, Magurele, Romania, and Institut National de la Santé et de la Recherche Médicale U33, Hôpital Bicêtre, Le Kremlin-Bicêtre, France

Received April 23, 1996; Revised Manuscript Received June 17, 1996[⊗]

ABSTRACT: FKBP59 is a protein usually associated with heat-shock protein hsp90 and steroid receptors. The N-terminal domain of the rabbit liver protein (149 amino acids) has a sequence homology with FKBP12, binds FK506 immunosuppressor, and has a peptidyl−prolyl *cis*−*trans* isomerase activity. The three-dimensional structure of this domain (FKBP59-I) was determined using homo- and heteronuclear multidimensional NMR spectroscopy, distance geometry, and molecular dynamics methods. Structure calculations used 1290 interproton distance restraints derived from nuclear Overhauser enhancement measurements, 29 dihedral ϕ angle restraints, and 92 hydrogen bond restraints. For the final 22 structures, the root mean square distance from the mean atomic coordinates, calculated for well-defined secondary structure fragments, is 0.47 ± 0.05 and 1.26 ± 0.15 Å for backbone heavy atoms (N, Cα, C′) and for all non-hydrogen atoms, respectively. The global fold contains a twisted six-stranded antiparallel β-sheet and a short α-helix packed on the hydrophobic side of the sheet. The 20 N-terminal and 12 C-terminal amino acids of the domain are disordered. The main-chain structure of FKBP59-I is globally similar to the NMR-derived and X-ray structures of unbound FKBP12. An unusual hydrogen bond interaction between the indole amino proton of Trp 89 and the aromatic cycle of Phe 129 was observed. This gives a large upfield shift (−4.8 ppm) and a significant exchange protection factor. The implications of the present structure determination on the ligand binding of FKBP59 are discussed.

FKBP59[1] (equally known as hsp56 or FKBP52) is a 59 kDa protein found in various animal tissues, associated with heat-shock protein hsp90 and steroid receptors in the absence of hormone (Renoir et al., 1990, Tai et al., 1986, 1992). It binds the potent immunosuppressant FK506 and has peptidyl−prolyl *cis*−*trans* isomerase (PPIase) activity. Cloning and sequencing the rabbit liver cDNA led to identification of an N-terminal region having a high sequence identity (52% over a common sequence of 107 amino acids) with the human FKBP12 immunophilin (Lebeau et al., 1992). Empirical structure prediction methods suggested that the protein has a modular organization made up of three immunophilin-like domains and a C-terminal tail (Callebaut et al., 1992). Moreover, overexpression and purification of the polypeptide corresponding to the first 149 N-terminal residues allowed to demonstrate that this first domain is indeed responsible for the immunosuppressor binding and the PPIase activity of the whole protein (Chambraud et al., 1993). However, despite the high sequence similarity and the conservation of the amino acid residues involved in ligand binding, the affinity for FK506 and rapamycin is decreased by about 2 orders of magnitude (Tai et al., 1992; Renoir et al., 1994). In addition, the complex with FK506 does not inhibit calcineurin phosphatase activity, as would be necessary for immunosuppressive activity (Lebeau et al., 1994). On the other hand, the precise biological function of FKBP59 is still not clearly established, although its association with steroid receptors and heat-shock proteins suggests that it may play a role in the modulation of the transcriptional control of glucocorticoid steroid and progesterone receptors (Tai et al., 1994; Renoir et al., 1995). By its isomerase activity, it may contribute to the proper folding of proteins in the cell (Schmid, 1991).

Understanding of the known functional features or of any other new activities which might emerge requires a detailed structural characterization of the protein and the study of molecular interactions with its cognate ligands. No crystallographic structure of the free FKBP59 or of its isolated domains is presently available, and by analogy with the previously studied immunophilins, the crystallization of the free form should be difficult. We therefore initiated an NMR project aiming to determine the three-dimensional structure and interaction properties of the N-terminal domain of FKBP59, which we called FKBP59-I. The domain was overexpressed in *Escherichia coli*, uniformly ^{15}N-labeled, and

[†] Supported by the Centre National de la Recherche Scientifique, the Institut National de la Santé et de la Recherche Médicale, the Institut Curie, and Rhône-Poulenc-Rorer (Bio-Avenir grant).

[‡] Coordinates have been deposited in the Brookhaven Protein Data Bank under the file names 1rou and 1rot.

* Address correspondence to this author at INSERM U350, Institut Curie, Centre Universitaire, Bâtiment 110-112, F-91405 Orsay, France. Fax: 33 1 69 07 53 27. E-mail: craescu@curie.u-psud.fr.

[§] INSERM U350.

[⊥] University of Bucarest.

[||] INSERM U33.

[⊗] Abstract published in *Advance ACS Abstracts,* August 1, 1996.

[1] Abbreviations: 2D, two dimensional; 3D, three dimensional; FKBP12, 12 kDa FK506 binding protein; FKBP59, 59 kDa FK506 binding protein; FKBP59-I, N-terminal domain (149 residues) of FKBP59; HMQC, heteronuclear multiple-quantum correlation spectroscopy; NOESY, nuclear Overhauser effect spectroscopy; PPIase, peptidyl−prolyl *cis*−*trans* isomerase; ppm, parts per million; rmsd, root mean square deviation.

S0006-2960(96)00975-0 CCC: $12.00

purified in our laboratories. In a previous paper we reported the ^1H and ^{15}N assignment of the NMR spectrum and described the secondary structure and the global folding of the free protein (Rouvière-Fourmy et al., 1995). These results provided the starting basis for the building of the three-dimensional structure using NMR restraints, distance geometry, and molecular dynamics methods. This paper describes the high-resolution three-dimensional structure of FKBP59-I in solution and discusses the main functional consequences. The structure of FKBP59-I is compared to the human and bovine FKBP12 determined by NMR and X-ray, respectively, and also to the X-ray structure of human FKBP12 in complex with an immunosuppressant drug.

MATERIALS AND METHODS

Sample Preparation. Overexpression in *E. coli*, ^{15}N labeling, and purification of FKBP59-I were described in a previous paper (Rouvière-Fourmy et al., 1995). NMR samples (1−2 mM) were prepared in 50 mM sodium phosphate buffer, pH 6.7, in 95% ^1H_2O/5% ^2H_2O or in ^2H_2O.

Experimental Restraints. The NMR data were collected on a Varian Unity 500 NMR spectrometer and processed on Silicon Graphics IRIS workstations. NOE distance restraints were collected from a 3D NOESY-HMQC spectrum (recorded in ^1H_2O, mixing time 100 ms) and a 2D NOESY spectrum (recorded in ^2H_2O, mixing time 150 ms). Peak picking, volume integrals, and calibration (volume to distance conversion) were performed using FELIX 2.3 software (Biosym Technologies, San Diego). Calibration of the volumes in the 3D spectrum used the $d_{\alpha N}(i,i+1)$ NOEs in the β-strands which correspond to a standard value of 2.2 Å. For the calibration of peak volumes in the 2D NOESY spectrum we used the $d_{\alpha\alpha}(i,j)$ interstrand NOE peaks, which in antiparallel β-sheets correspond to 2.3 Å (Wüthrich, 1986). The distance NOE constraints were defined as strong (1.8−2.8 Å), medium (2.8−3.5 Å), and weak (3.5−5.0 Å). Pseudoatom corrections were made using the classes and upper-bound restraint corrections proposed by Wüthrich et al. (1983). A total of 1290 NOE distance restraints were used (Table 1). Of these, 320 (24.8%) represent intraresidue NOEs, 403 (31.2%) were sequential NOEs, 161 (12.5%) were from short-range NOEs ($|i - j| < 5$), and 406 (31.4%) were from long-range NOEs.

Hydrogen bonds were identified from $^1H/^2H$ exchange experiments and were included as pairs of restraints between NH and N atoms to the corresponding carbonyl O atom but only when NOE patterns indicated unambiguously donor acceptor pairs (Rouvière-Fourmy et al., 1995). The 92 restraints were thus included, defining the O−N distance between 2.8 and 3.3 Å and the O−H distance to be between 1.8 and 2.3 Å.

The vicinal coupling constant were determined from *J*-modulated HMQC experiments (Kuboniwa et al., 1994) in which the jump and return sequence for water elimination was replaced by a selective presaturation. A total of 29 dihedral restraints were derived using the following relationships: for $^3J_{NH\alpha} < 6$ Hz, $\phi = -50 \pm 40°$, and for $^3J_{NH\alpha} > 9$ Hz, $\phi = -120 \pm 40°$.

Structure Calculation. A hybrid distance geometry/simulated annealing procedure was used for structure generation [using the DGII program (Havel, T. F. (1991)] and refinement under NMR restraints (Nilges et al., 1989).

The 37 structures thus obtained were subjected to a simulated annealing protocol using the Discover program (Biosym Technologies, San Diego) and the consistent valence force field, completed with potential energy terms for the distance and dihedral angle restraints. The protocol followed essentially that proposed by Gippert et al. (1990). Before dynamics, structures were energy minimized using 3000 iterations of conjugated gradient algorithm with a force constant for the NOE restraint energy term (k_{NOE}) equal to 1 kcal/(mol·Å^2). The system was then heated to 1200 K in several steps during 3 ps with a simultaneous progressive increase of k_{NOE} from 1 to 32 kcal/(mol·Å^2). The 3 ps equilibration phase was followed by a 6 ps annealing procedure under constant distance restraints. At the end of dynamics, the molecules were subjected to 3000 cycles of steepest descent and 3000 cycles of conjugate gradient energy minimization.

Twenty-two refined structures were finally retained on the basis of potential energy and restraint violation analysis. This ensemble was further used for statistical and structural characterization of the protein three-dimensional structure. The restrained minimized average structure was obtained by averaging the atomic coordinates of the superposed individual structures and subjecting the resulting coordinates to energy minimization under experimental restraints. Calculations were performed on Silicon Graphics 4D/35 and 4D/280 workstations.

$^1H/^2H$ exchange rates were estimated from the analysis of successive HMQC spectra recorded after the lyophilized sample was dissolved in ^2H_2O. The data points were fitted using a simple exponential function. For some rapidly decaying cross-peaks (I24, V32, K34, K37, L38, M47, D50, D90, V98, I121, A125, and F134) estimated low-limit values were attributed. Finally, 51 (42% of those representing the well-organized structure) amide proton exchange rates could be obtained. In order to evaluate more accurately the contribution of secondary and tertiary structure to the decrease in amide hydrogen exchange, we calculated the protection factors (*P*) using the formula (Molday et al., 1972; Bai et al., 1993):

$$P = K_{rc}/K_{ex}$$

where K_{rc} is the exchange rate in a random coil conformation and K_{ex} is the actual measured rate. Accurate values for K_{rc} were recently determined (Bai et al., 1993) to take into account the influence of the local sequence, temperature, pH, and salt concentration. In our conditions ($pD_{corr} = 7.2$, $T =$ 308 K, low salt concentration) the acidic and neutral contributions are negligible as compared to the base-catalyzed term.

RESULTS AND DISCUSSION

Experimental Restraints. The distribution of the NOE restraints used in the present structural determination is shown in Figure 1. Two clear features can be noted. The first 20 and the last 11 residues in the sequence are practically devoid of long-range NOE interactions, and the sequential NOEs are weaker than in the core of the protein. Further, the intraresidue correlation peaks (COSY, TOCSY) are stronger and show a smaller line width. These observations indicate high flexibility and irregular structures, as was noted previously in the assignment stage (Rouvière-Fourmy et al.,

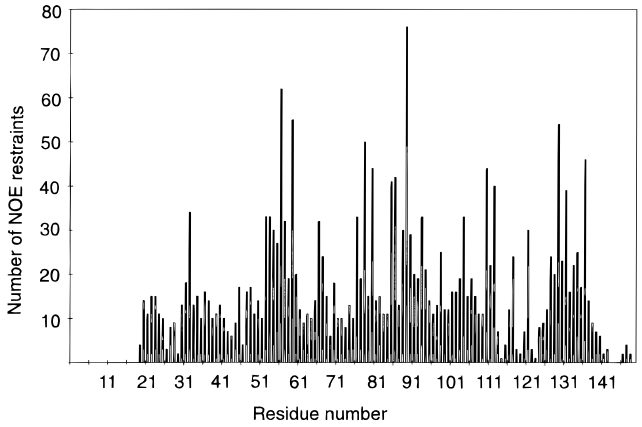

FIGURE 1: Plot of the number of NOE distance restraints for each residue in the sequence. All interresidue restraints appear twice, once for each of the two interacting residues. The restraints were classified (represented from bottom to top) as intraresidue, sequential, medium range, and long range ($|i - j| \geq 5$).

Table 1: Structural Statistics for the 22 Simulated Annealing Structures of FKBP59-I[a]

restraint statistics	
NOE restraints	1290
intraresidue	320 (24.8%)
sequential	403 (31.2%)
medium range	161 (12.5%)
long range ($\|i - j\| > 5$)	406 (31.4%)
dihedral angle restraints	29
hydrogen bond restraints	92
av no. of NOE restraint violations	
larger than 0.5 Å	none
between 0.4 and 0.5 Å	2.1
between 0.3 and 0.4 Å	10.5
between 0.2 and 0.3 Å	45.6

structural statistics (rmsd)[b]	av pairwise rmsd (Å)	av rmsd (Å) from the av structure
backbone	0.60 ± 0.08	0.47 ± 0.05
heavy atoms	1.68 ± 0.19	1.26 ± 0.15

[a] The mean atomic root mean square deviations were calculated after superposition of the backbone heavy atoms (N, Cα, C′) in well-defined secondary structure fragments. [b] The fragments used for calculating rmsds are 32−37, 50−60, 64−68, 76−80, 87−95, 101−107, and 127−137.

1995). Therefore, the present structural analysis will be limited to fragment 21−138. The mean number of NOE restraints per residue in this fragment is about 11, representing a reasonable experimental basis for generating a reliable NMR structure. Second, the restraint distribution is not homogeneous over the sequence: the β-strands and the α-helix show considerably more restraints than the turns and loops. In particular, the aromatic side chains forming a hydrophobic core have the largest number of restraints.

Quality of the Structures. Table 1 gives an evaluation of the quality and precision of structure determination. None of the structures showed NOE violations larger than 0.5 Å, and the average number of NOE restraint violations larger than 0.4 Å is 2.1. Generally, there is a close correlation between the definition of the structure in a certain region and the number of restraints involving the residues of that region. Figure 2 shows the final 22 energy-refined structures, superimposed for best fit on backbone atoms (N, Cα, C′) in well-defined secondary structures. It enables a straightforward visualization of the quality of generated structures. As usual, the core of the molecule is well determined and gives a good superposition, in contrast with the solvent-exposed sites (turns or loops) where the structure is more flexible.

The final family of 22 structures has an average pairwise root mean square deviation of 0.60 ± 0.08 and 1.68 ± 0.19 Å for the backbone and all heavy atoms, respectively, involved in well-defined secondary structures (fragments 32−37, 50−60, 64−68, 76−80, 87−95, 101−107, and 127−137). These values fall down to 0.47 ± 0.05 and 1.26 ± 0.15 Å when the rmsds are calculated relative to the average structure. Such values are typical for high-resolution NMR structures.

An efficient assessment of the structure quality may be obtained from the Ramachandran plot for the dihedral backbone angles. As may be seen in Figure 3, which corresponds to the minimized average structure, 93% of the ϕ/ψ pairs lie within energetically allowed two-dimensional regions and only two residues (Lys 73 and Glu 84) have an unfavored geometry. The mean number of residues located in disallowed regions of the Ramachandran plot for individual refined structures is 2.6. Lys 73 and Glu 84 are the most encountered (in 68% and 27% of the structures, respectively). Lys 73 belongs to a flexible, large β-bulge while Glu 84 is situated in a better defined region. In this last case, the positive ϕ angle is compatible with the measured $^3J_{NH\alpha}$ coupling constant (6.5 Hz). In fact, according to the Karplus equation, this coupling constant value may be associated with both positive and negative ϕ angles. The coupling constant could not be measured for Lys 73.

We used the Procheck program (Morris et al., 1992) for a more complete evaluation of the stereochemical quality of the obtained structures. Based on a systematic check of several structural parameters (ϕ/ψ distribution, pooled χ_1 standard deviations, and hydrogen bond donor energies), the program allows a classification of a given structure in four classes (the quality decreases from class 1 to class 4). According to this analysis, the energy-minimized average structure of FKBP59-I belongs to class 2, which includes a large number of X-ray structures.

Structure Description. The structure consists mainly of a six-stranded antiparallel β-sheet with hairpin connections, having a right-handed twist and a well-defined amphiphilic character (Figure 4). The β-strands are defined by the following amino acids: (B1) 22−24, (B2) 32−37, (B3) 50−60, (B4a) 64−68, (B4b) 76−80, (B5) 101−107, and (B6) 127−137. Two classical β-bulges (F66 in strand B4a and E135 in strand B6) and a larger one between strands B4a and B4b were observed. Despite its high conformational flexibility, the N-terminal strand (B1) was clearly identified by several criteria including secondary shifts of Cα protons, strong $d_{\alpha N}(i,i+1)$ NOE connectivities, interstrand contacts, and slow exchange of amide protons in Ile 24, Val 32, and Lys 34 (Rouvière-Fourmy et al., 1995). The hydrophobic, concave side of the β-sheet is wrapped around a short, hydrophobic α-helix (87−95) which connects strands B4 and B5. Two classical, relatively well-defined β-turns were identified, a type I (60−63) and a type II (47−50). Two other type II β-turns, situated between the α-helix and strand B5 (97−100) and in the large loop between strands B5 and B6 (117−120), are more disordered. The largest loop from 108 to 126 is poorly defined, reflecting the small number of structural restraints in this region (Figure 1). Nevertheless, the small N-side fragment of the loop (108−113) is better

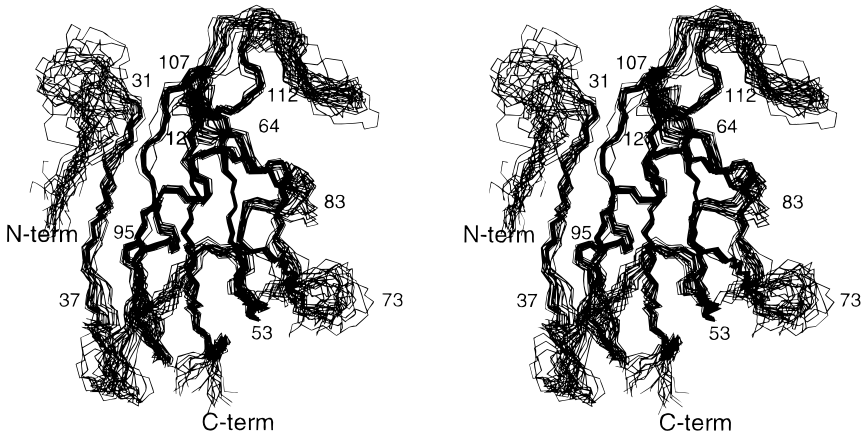

FIGURE 2: Stereoview of the 22 superimposed final structures of FKBP59-I, represented by the backbone heavy atoms (N, Cα, C′) of residues 21−138. The conformers are shown with the N-terminus at the left and the C-terminus below.

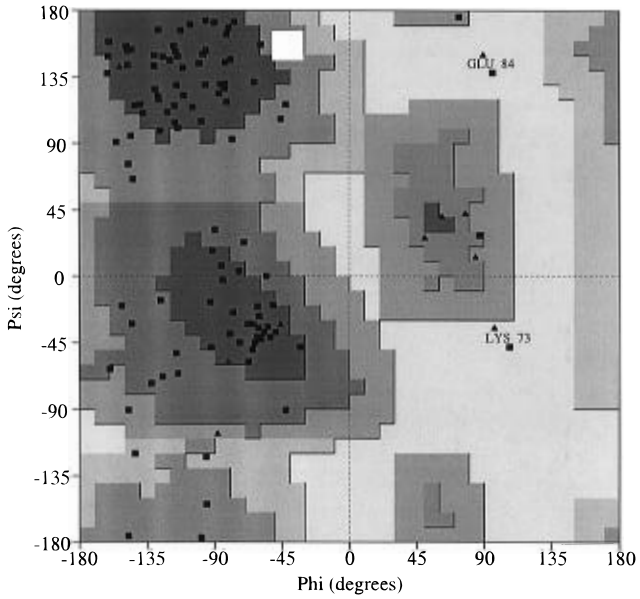

FIGURE 3: Ramachandran plot (drawn using the PROCHECK package) for the energy-minimized average structure of FKBP59-I. Glycine residues are indicated by triangles. The two labeled amino acids have ϕ/ψ angles in a disallowed two-dimensional region.

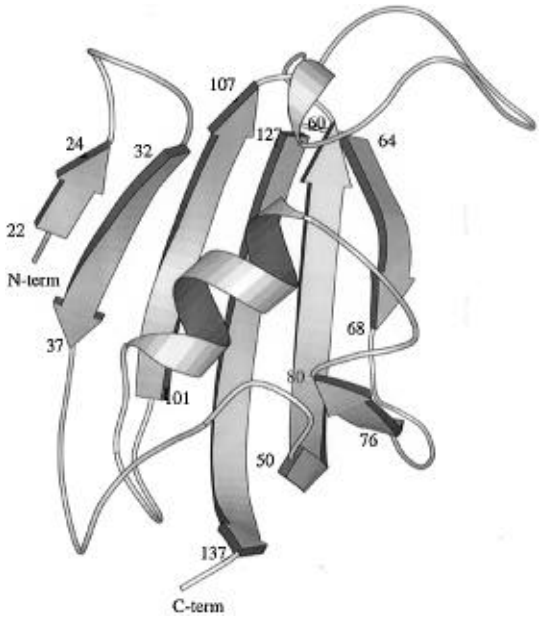

FIGURE 4: Schematic drawing of the three-dimensional structure of FKBP59-I. The energy-minimized average structure was used in the MOLSCRIPT software (Kraulis, 1991).

defined and includes a single-turn 3_{10} helix (108−110) and a small loop. A hydrogen bond between the carbonyl oxygen of Pro 108 and the amide proton of Gly 113, observed in all the final structures, should play an important role in the stability of this region.

The β-sheet presents a particular folding topology (+1, +3, +1, −3, +1), which differs only by an additional N-terminal strand from that described in human and bovine FKBP12 (Michnick et al., 1991; Moore et al., 1991). The interesting feature of this topology is the presence of a loop crossing (between loops 38−50 and 96−100) requiring precise interchain polar interactions. Analysis of the present structures shows that two hydrogen bonds between the main-chain atoms in the two loops are possible: HN(98) → O (44) and HN(41) → O(98). The first hydrogen bond is stable enough to induce a significant protection against ^{2}H exchange (see later). Other additional interloop interactions, observed in liganded FKBP12 (Michnick et al., 1991; Van Duyne et al., 1993; Meadows et al., 1993), involving Ser 67 and Thr 14 are not possible in FKBP59-I where these residues are substituted by a Lys and a Glu, respectively.

FKBP59-I contains two Cys residues, both in strand B5 (Cys 102 and Cys 106). One of the Cys residues (Cys 106) replaces a larger size, highly conserved Ile residue in the FKBP family. Simultaneously, in front of this position, an Ala residue on the α-helix (Ala 88) replaces a Gly, another well-conserved amino acid (Galat & Metcalfe, 1995). Both Cys side chains are situated on the internal, hydrophobic side of the β-sheet and have low solvent accessibility. Usually, the $S_\gamma H$ protons of Cys residues are not observed in NMR spectra due to their rapid exchange with the solvent. In the present case, observation of these exchangeable protons in the two cysteines (Rouvière-Fourmy et al., 1995) suggests that the thiol groups participate in hydrogen bonds as proton donors. Analysis of the calculated structures shows that the most probable hydrogen acceptors are the carbonyl oxygen of Leu 101 and of Leu 127 for Cys 102 and Cys 106, respectively. Together with the structural burial in a hydrophobic environment, these hydrogen bonds may explain the high stability against oxidation of the Cys residues during the experimental manipulations.

Amide−Aromatic Hydrogen Bond. The $N_{\epsilon 1}$ proton in Trp 89 has an unusual chemical shift value (Rouvière-Fourmy

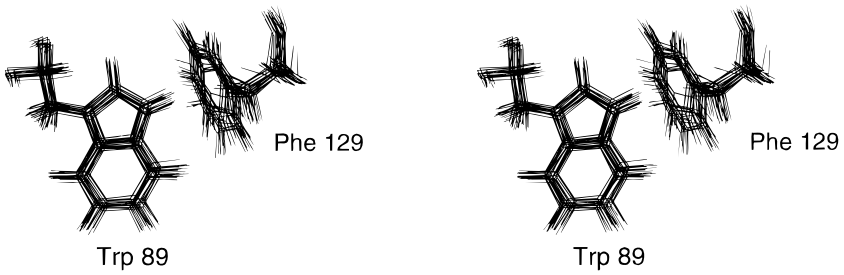

FIGURE 5: Stereoview of the two residues (Trp 89 and Phe 129) involved in an amino−aromatic hydrogen bond. Side chains are shown for the 22 final structures after superimposing the backbone heavy atoms in well-defined secondary fragments.

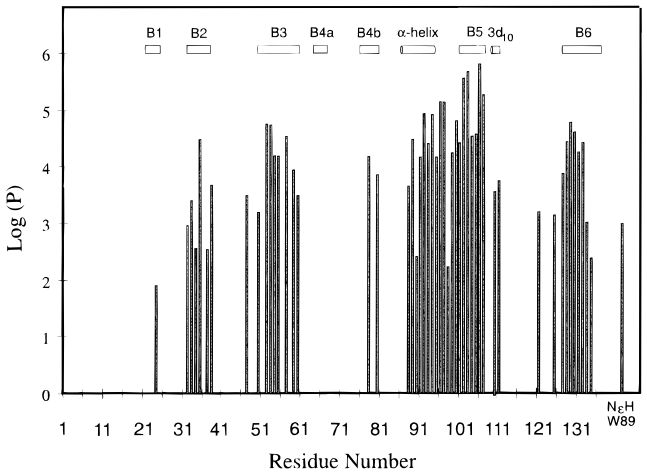

FIGURE 6: Plot of the protection factors for the amide proton exchange in FKBP59-I in phosphate buffer (50 mM), pH 6.7, at 308 K.

et al., 1995) which represents about a 4.8 ppm upfield shift relative to the random coil position (Wüthrich, 1986). Its assignment is consistent with all the COSY, TOCSY, and NOESY connectivities and is further confirmed by the coupling constant (proton coupling $N_{\epsilon 1}H/C_{\delta 1}H = 2.5$ Hz) which is significantly lower than for any amide proton. Inspection of the three-dimensional structure shows that the amino proton lies over the aromatic cycle of Phe 129, close to the ring center (2.53 Å) (Figure 5). Ring current shift calculations, using the Johnson−Bovey model (Johnson & Bovey, 1958) with the calibrations of Cross and Wright (1985) and the energy-minimized average structure, are able to explain only half (2.61 ppm) of the total observed upfield shift. The other half of the shielding effect could originate from other electronic factors, including the chemical nature of the proton donor, bond-polarization effects, and an electronic charge transfer from the proton acceptor [Deakyne, & Meot-Ner (Mautner), 1985]. A comparable discrepancy between the calculated and observed shielding effect was observed for a primary amino and an amide proton lying close to a Tyr ring in bovine pancreatic trypsin inhibitor (Tücsen & Woodward, 1987).

The Trp 89 $N_{\epsilon 1}H$ group shows a second interesting feature: its isotope exchange rate is considerably decreased. The calculated protection factor (Figure 6) is of the same order of magnitude as the amide protons involved in some interstrand hydrogen bonds. Together, these two properties strongly indicate that the Trp 89 $N_{\epsilon 1}H$ and Phe 129 ring form an amino−aromatic unconventional hydrogen bond in which the aromatic group is the proton acceptor. Analysis of high-resolution protein crystal structures (Burley & Petsko, 1986) and energy calculations (Levitt & Perutz, 1988) have indeed shown that amide backbone protons or side-chain amino groups may interact (mainly electrostatically) with aromatic systems. In some cases the proton donor and acceptor groups may be part of two interacting species like in hemoglobin−drug (Perutz et al., 1986) SH2−phosphotyrosine (Waksmann et al., 1993), or acetylcholine esterase−substrate (Sussman et al., 1991) complexes. The enthalpy contribution of such an interaction in various models was theoretically estimated to be roughly half of that corresponding to intraprotein hydrogen bonds [Deakyne, & Meot-Ner (Mautner), 1985; Levitt & Perutz, 1988; Rodham et al., 1993], in good agreement with the slow exchange rate observed here.

Both Trp 89 and Phe 129 are directly involved in the ligand binding as shown by the analysis of NMR spectra of liganded (FK506) protein (Rouvière and Craescu, unpublished results) and are perfectly conserved in the series of FK506-binding proteins (Galat & Metcalfe, 1995). Therefore, besides a contribution to the structural stability, their amino−aromatic interaction may play a role in the affinity and specificity control of the ligand binding.

The particular geometry, described here for the Trp 89/Phe 129, is highly similar to that observed for the corresponding Trp 59/Phe 99 in FKBP12 structures derived by NMR (Michnick et al., 1991; Meadows et al., 1993) or X-ray methods (Van Duyne et al., 1993). Unfortunately, we were not able to compare the magnetic shielding effect on the $N_{\epsilon 1}$ proton because its assignment was not reported in the paper of Xu et al. (1993) and is probably erroneous in the paper of Rosen et al. (1991). In fact, the chemical shift value, proposed in this last report, would suggest that it contains no significant ring current contribution, in contradiction with the calculated structure.

Dynamics. In given physicochemical conditions (pH, temperature, salts, etc.) the study of amide hydrogen exchange can provide information about high-energy conformational fluctuations at various levels of structural organization. For reliable quantitative analysis of these results the observed exchange rates must be referenced to the intrinsic values, measured in an unfolded state. The factors thus obtained, called the protection factors (*P*), measure the influence of the native structure on the dynamics controlling the exchange process (Molday et al., 1972; Bai et al., 1993; Kragelund et al., 1995).

Figure 6 presents a histogram of the protection factors of the amide protons against residue number in FKBP59-I. The values vary between 80 (Ile 24) and 6.0×10^5 (Cys 106) as in the case of other proteins studied by NMR (Jeng et al., 1990; Jeng & Englander, 1991; Kragelund et al., 1995; Jeng & Dyson, 1995). The slow exchange rates were generally found in helices and β-sheet secondary structures in which the amide protons participate to specific hydrogen bonds.

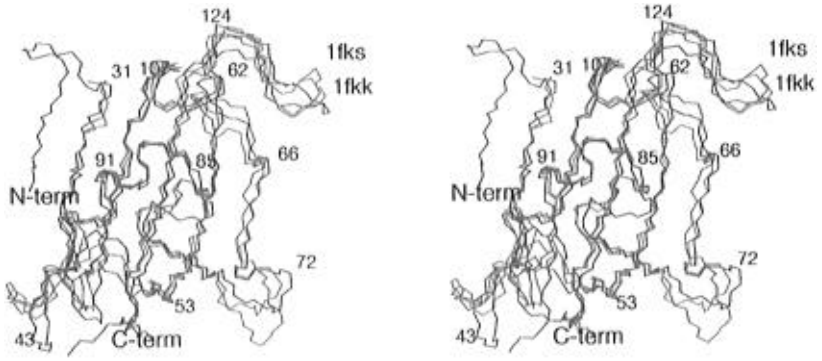

FIGURE 7: Stereo plot of the superimposed backbone structures of FKBP59-I (the energy-minimized average structure, in blue) and the NMR (red) and X-ray (green) structures of FKBP12. The backbone atoms (N, Cα, C′) in segments 32−37, 50−60, 64−68, 76−80, 87−95, 101−107, and 127−137 (amino acid numbers of FKBP59-I) were used for the best fit.

The solvent accessibility and the local or regional conformational flexibility are additional factors modulating the exchange process (Englander et al., 1996).

As resulting from Figure 5, the major part of the exchange-protected amide protons belongs to well-determined secondary structure elements. The protection factors are higher in the inner β-strands (B3, B5, and B6) and the α-helix and are lower in the peripheral strands (B1, B2, and B4) which are more exposed to the solvent. According to the exchange data, the first part of the B4 strand is considerably more flexible than the second part, in agreement with the smaller number of NOE restraints (Figure 1) and a poor superposition of the final structures in this region (Figure 2). More generally, agreement between the protection factors, relative number of restraints, and the rmsds is strong evidence that the conformational variability in a given region may be regarded as reliable and reflects an intrinsic property of the structure and not an experimental artifact.

Recently, comparison of 19 different crystallographic structures of the free and liganded FKBP12s (Wilson et al., 1995) pointed out the existence of regions having a larger variation in structure, suggesting that they originate from a higher local mobility. In particular, the difference in structural definition between the two segments of strand B4 observed here is in good agreement with the rmsd distribution in the corresponding fragments (B3a and B3b in FKBP12) of the crystallographic structures.

Comparison with Other Immunophilin Structures. There are two three-dimensional structures of free FKBP12 obtained by NMR (Moore et al., 1991; Michnick et al., 1991), but only one of them is available in the Protein Data Bank. The crystallographic structure of the unliganded bovine FKBP12 has only been solved recently (Wilson et al., 1995); the difficulty in sample crystallization and the poor diffraction of the crystals are probably related to the higher flexibility of the uncomplexed protein.

Figure 7 shows the best superposition between the FKBP59-I and the unliganded structures of FKBP12 solved by X-ray and NMR spectroscopy (PDB entries 1fkk and 1fks, respectively). As seen in the figure, there is a high degree of similarity between the three structures. The rmsds calculated for the heavy atoms in well-resolved secondary structure elements are 1.00 Å for 1fkk and 1.28 Å for 1fks. This means that there is a greater similarity with the X-ray structure of FKBP12. The difference is probably due to the lower definition of the previous NMR structures rather than to a real conformational change between solution and crystal states. FKBP59-I is also very similar to the structure of FKBP12 in complex with FK506 (Van Duyne et al., 1993) (the rmsd with 1fkf is 1.04 Å), in agreement with the observation that complexation does not change significantly the overall structure of the immunophilin (Van Duyne et al., 1993; Wilson et al., 1995).

Globally, the number and delimitations of the secondary structure elements observed in the present work for FKBP59-I are similar to that previously reported for the free FKBP12 (Moore et al., 1991; Michnick et al., 1991; Wilson et al., 1995). The main difference is the presence of a sixth β-strand at the N-terminal side of FKBP59-I, which has no counterpart in the sequence of human and bovine FKBP12. A similar short β-strand on the N-terminal side was only observed in the crystal structure of the liganded yeast FKBP12 (Rotonda et al., 1993). However, the increase in the width of the β-sheet, due to the additional β-strand, is unlikely to affect the functional properties of the protein. Thus, the FKBP13 structure, which has only four strands (due to the absence or disorder of the N-terminal β-strand), is still able to bind tightly the immunosuppressor (Schultz et al., 1994).

Other differences appear at a closer inspection of the common part of the structures. Thus, the first part of strand B4 (64−68) and the 3_{10} helix were not identified in any of the NMR structures of free FKBP12 (Moore et al., 1991; Michnick et al., 1991) while the second part of strand B6 (124−127) was only observed in the report of Michnick et al. (1991). The present results and the recent X-ray structure of unliganded human FKBP12 (Wilson et al., 1995) strongly suggest that these structural differences are not real but reflect a reduced number of NMR parameters used in the previous NMR studies in defining the secondary structure elements. Larger structural variations may be observed in the irregular fragments, like the β-bulge between Ser 69 and Lys 75 and loops Arg 38−Gly 49 and Gly 81−Ile 86 (Figure 7). This reflects the smaller number of experimental restraints and the consequently larger dispersion of the calculated structures (Figure 2).

Functional Implications. FKBP59 is able to bind the immunosuppressant drugs (FK506 and rapamycin) but with a lower binding constant (about 2 orders of magnitude) as compared to FKBP12 (Tai et al., 1992; Renoir et al., 1994). The complex formed with FK506 does not inhibit significantly the phosphatase activity of calcineurin (Peattie et al., 1992; Wiederrecht et al., 1992; Lebeau et al., 1994). The presently determined three-dimensional structure of the

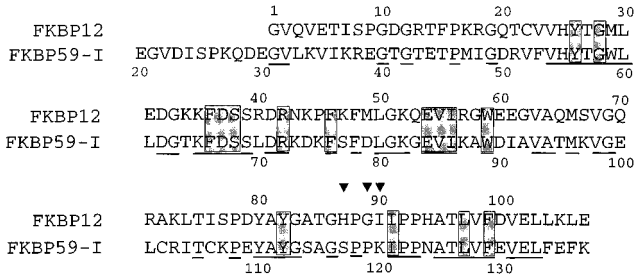

FIGURE 8: Sequence comparison FKBP59-I−human FKBP12: Underlines, conserved residues; boxes, amino acids involved in ligand binding; arrows, amino acid differences which may be responsible for functional changes.

FKBP59-I domain could help us to explain some of the binding properties. The overall high similarity with the solution or X-ray structures of FKBP12, in particular, the conservation of the hydrophobic pocket delimited by the β-sheet and the α-helix, is in good agreement with the conservation of immunosuppressor binding capacity.

Analysis of the FKBP12−ligand complexes (Meadows et al., 1993; Orozco et al., 1993; Van Duyne et al., 1993) and site-directed mutagenesis experiments (Futer et al., 1995) allowed us to identify about 15 amino acids directly involved in interactions with the drugs or with pro-containing small peptides. They are located in the hydrophobic pocket and in two flexible loops (68−76 and 113−126) surrounding the entrance to the pocket. As results from primary structure comparison, all these residues are identical or conservatively substituted in the FKBP family, including FKBP59-I (Figure 8). It appeared that the critical amino acid substitutions which may modulate the ligand binding are essentially localized in the flexible regions (Clardy, 1995), particularly in loop 113−126. Thus, substitution of Gly 89 by a Pro in FKBP12 decreases the affinity for FK506 by a factor of 7: K_i for PPIase inhibition changes from 0.4 ± 0.2 to 2.7 ± 0.8 nM (Yang et al., 1993). This mutation corresponds precisely to one of the differences in primary structure between FKBP12 and FKBP59-I (Figure 8) and may partially explain the lower affinity of FKBP59-I for the ligand. Unfortunately, the literature data on the Ile 90 to Lys substitution are contradictory: it was reported to induce a 4-fold increase in FK506 binding by Yang et al. (1993) but a 4-fold decrease by Futer et al. (1995). The situation is more complex when calcineurin inhibition is considered: while the ligand binding of the double mutant of FKBP12 (Gly89Pro and Ile90Lys) is normal, the inhibition of the phosphatase activity is practically lost (reduced by a factor of 600).

The case of His 87 (in FKBP12) is somewhat more complicated: its substitution by different amino acids results in various effects ranging from no effect (Val, Phe) to a 3-fold (Ala) and 40-fold (Leu) decrease in binding affinity (Aldape et al., 1992; Futer et al., 1995). Inhibition of the phosphatase activity decreased to a smaller extent (from 1 to 4 times). Therefore, we can reasonably assume that the presence of three amino acids (Ser 117, Pro 119, and Lys 120; see Figure 8) in FKBP59-I represents the minimal substitutions (relative to the FKBP12) responsible for the lack of calcineurin inhibition. However, the change in ligand affinity must be the cumulative result of various amino acid substitutions in the whole binding pocket. A more clear picture of the structure−function relationships requires additional spectroscopic studies on the protein−ligand interactions and dynamics. These experiments are currently under way in our laboratory.

Conclusion. The present study of a domain, isolated from FKBP59, further demonstrates the utility of the strategy consisting of isolation and independent structure determination of modules from larger proteins. We showed that the N-terminal domain may be separately expressed in *E. coli*, is highly stable, and has a well-defined three-dimensional fold. Moreover, as the protein's known ligands, FK506 and rapamycin, are macrolides of fungal origin and obviously not the physiological effectors of FKBP59, a better comprehension of its three-dimensional structure is important for the search of endogenous molecules which bind to FKBP59-I and eventually for the identification of its cellular target. This will help us to understand the cellular function-(s) of FKBP59 and its (their) regulation.

ACKNOWLEDGMENT

We thank E. Quiniou for advice on computing.

REFERENCES

Aldape, R. A., Futer, O., DeCenzo, M. T., Jarrett, B. P., Murcko, M. A., & Livingston, D. L. (1992) *J. Biol. Chem. 267*, 16029−16032.
Bai, Y., Milene, S. J., Mayne, L., & Englander, S. W. (1993) *Proteins: Struct., Funct., Genet. 17*, 75−86.
Burley, S. K., & Petsko, G. A. (1986) *FEBS Lett. 203*, 139−143.
Callebaut, I., Renoir, J.-M., Lebeau, M.-C., Massol, N., Burny, A., Baulieu, E.-E., & Mornon, J. P. (1992) *Proc. Natl. Acad. Sci. U.S.A. 89*, 6270−6274.
Chambraud, B., Rouvière-Fourmy, N., Radanyi, C., Hsiao, K., Peattie, D. A., Livingston, D. J., & Baulieu, E.-E. (1993) *Biochem. Biophys. Res. Commun. 196*, 160−166.
Clardy, J. (1995) *Proc. Natl. Acad. Sci. U.S.A. 92*, 56−61.
Cross, K. J., & Wright, P. E. (1985) *J. Magn. Reson. 64*, 220−231.
Deakyne, C. A., & Meot-Ner (Mautner), M. (1985) *J. Am. Chem. Soc. 107*, 474−479.
Englander, S. W., Sosnick, T. R., Englander, J. J., & Mayne, L. (1996) *Curr. Opin. Struct. Biol. 6*, 18−23.
Futer, O., DeCenzo, M. T., Aldape, R. A., & Livingston, D. J. (1995) *J. Biol. Chem. 270*, 18935−18940.
Galat, A., & Metcalfe, S. M. (1955) *Prog. Biophys. Mol. Biol. 63*, 69−119.
Gippert, G. P., Yip, P. F., Wright, P. E., & Case, D. A. (1990) *Biochem. Pharmacol. 40*, 15−22.
Havel, T. F. (1991) *Prog. Biophys. Mol. Biol. 56*, 43−78.
Jeng, M.-F., & Englander, S. W. (1991) *J. Mol. Biol. 221*, 1045−1061.
Jeng, M.-F., & Dyson, J. (1995) *Biochemistry 34*, 611−619.
Jeng, M.-F., Englander, S. W., Elöve, G. A., Wand, A. J., & Roder, H. (1990) *Biochemistry 29*, 10433−10437.
Johnson, C. E., & Bovey, F. A. (1958) *J. Chem. Phys. 29*, 1012−1014.
Kragelund, B. B., Knudsen, J., & Poulsen, F. M. (1995) *J. Mol. Biol. 250*, 695−706.
Kraulis, P. J. (1991) *J. Appl. Crystallogr. 24*, 946−950.
Kuboniwa, H., Grzesiek, S., Degaglio, F., & Bax, A., (1994) *J. Biomol. NMR 4*, 871−878.
Lebeau, M.-C., Massol, N., Herrick, J., Faber, L. E., Renoir, J.-M., Radanyi, C., & Baulieu, E.-E. (1992) *J. Biol. Chem. 267*, 4281−4284.
Lebeau, M.-C., Myagkikh, I., Rouvière-Fourmy, N., Baulieu, E.-E., & Klee, C. B. (1994) *Biochem. Biophys. Res. Commun. 203*, 750−755.
Levitt, M., & Perutz, M. F. (1988) *J. Mol. Biol. 201*, 751−754.
Meadows, R. P., Nettesheim, D. G., Xu, R. X., Olejniczak, E. T., Petros, A. M., Holzman, T. F., Severin, J., Gubbins, E., Smith, H., & Fesik, W. (1993) *Biochemistry 32*, 754−765.

Michnick, S. W., Rosen, M. K., Wandless, T. J., Karplus, M., & Schreiber, S. L. (1991) *Science 252*, 836−839.
Molday, R. S., Englander, S. W., & Kallen, R. G. (1972) *Biochemistry 11*, 150−158.
Moore, J. M., Peattie, D. A., Fitzgibbon, M. J., & Thomson, J. A. (1991) *Nature 351*, 248−250.
Morris, A. L., MacArthur, M. W., Hutchinson, E. G., & Thorntont, J. M. (1992) *Proteins: Struct., Funct., Genet. 12*, 345−364.
Nilges, M., Clore, G. M., & Gronenborn, A. M. (1989) *FEBS Lett. 229*, 317−324.
Orozco, M., Tirado-Rives, J., & Jorgensen, W. L. (1993) *Biochemistry 32*, 12864−12874.
Peattie, D. A., Harding, M. W., Fleming, M. A., DeCenzo, M. T., Lipke, J. A., Livingston, D. J., & Benasutti, M. (1992) *Proc. Natl. Acad. Sci. U.S.A. 89*, 10974−10978.
Perutz, M. F., Fermi, G., Abraham, D. J., Poyart, C., & Bursaux, E. (1986) *J. Am. Chem. Soc. 108*, 1064−1078.
Renoir, J.-M., Radanyi, C., Faber, L. E., & Baulieu, E.-E. (1990) *J. Biol. Chem. 265*, 10740−10745.
Renoir, J.-M., Le Bihan, S., Mercier-Bodard, C., Gold, A., Arjomandi, M., Radanyi, C., & Baulieu, E.-E. (1994) *J. Steroid Biochem. Mol. Biol. 48*, 101−110.
Renoir, J.-M., Mercier-Bodard, C., Hoffmann, K., LeBihan, S., Ning, Y.-M., Sanchez, E. R., Handschumacher, R. E., & Baulieu, E.-E. (1995) *Proc. Natl. Acad. Sci. U.S.A. 92*, 4977−4981.
Rodham, D. A., Suzuki, S., Suenram, R. D., Lovas, F. J., Dasgupta, S., Goddard, III, & Blake, G. A. (1993) *Nature 362*, 735−737.
Rosen, M. K., Michnick, S. W., Karplus, M., & Schreiber, S. L. (1991) *Biochemistry 30*, 4774−4789.
Rotonda, J., Burbaum, J. J., Chan, H. K., Marcy, A. I., & Becker, J. W. (1993) *J. Biol. Chem. 268*, 7607−7609.
Rouvière-Fourmy, N., Craescu, C. T., Mispelter, J., Lebeau, M.-C., & Baulieu, E.-E. (1995) *Eur. J. Biochem. 231*, 761−772.
Schmid, F. X. (1991) *Curr. Opin. Struct. Biol. 1*, 36−41.
Schultz, D., Martin, P. K., Lianf, J., Schreiber, S. L., & Clardy, J. (1994) *J. Am. Chem. Soc. 116*, 3129−3130.
Sussman, J. L., Harel, M., Frolow, F., Oefner, C., Goldman, A., Toker, L., & Silman, I. (1991) *Science 253*, 872−879.
Tai, P.-K. K., Maeda, Y., Nakao, K., Wakim, N. G., Duhring, J. L., & Faber, L. E. (1986) *Biochemistry 25*, 5269−5275.
Tai, P.-K. K., Albers, M. W., Chang, H., Faber, L. E., & Schreiber, S. L. (1992) *Science 256*, 1315−1318.
Tai, P.-K. K., Albers, M. W., McDonnell, D. P., Chang, H., Schreiber, S. L., & Faber, L. E. (1994) *Biochemistry 33*, 10666−10671.
Tüchsen, E., & Woodward, C. (1987) *Biochemistry 26*, 1918−1925.
Van Duyne, G. D., Standaert, R. F., Karplus, P. A., Schreiber, S. L., & Clardy, J. (1993) *J. Mol. Biol. 229*, 105−124.
Waksman, G., Kominos, D., Robertson, S. C., Pant, N., Baltimore, D., Birge, R. B., Cowborn, D., Hanafusa, H., Mayer, B. J., Overduin, M., Resh, M. D., Rios, C. B., Silverman, L., & Kuriyan, J. (1992) *Nature 358*, 646−653.
Wiederrecht, G., Hung, S., Chan, H. K., Marcy, A., Martin, M., Calaycay, J., Boulton, D., Sigal, N., Kincaid, R. L., & Siekierka, J. J. (1992) *J. Biol. Chem. 267*, 21753−21760.
Wilson, K. P., Yamashita, M. M., Sintchak, M. D., Rotstein, S. H., Murcko, M. A., Boger, J., Thomson, J. A., Fitzgibbon, M. J., Black, J. R., & Navia, M. A. (1995) *Acta Crystallogr. D51*, 511−521.
Wüthrich, K. (1986) *NMR of Proteins and Nucleic Acids*, John Wiley & Sons, New York.
Wüthrich, K., Billeter, M., & Braun, W. (1983) *J. Mol. Biol. 169*, 949−961.
Xu, R. X., Nettesheim, D., Olejniczak, E. T., Meadows, R., Gemmecker, G., & Fesik, S. W. (1993) *Biopolymers 33*, 535−550.
Yang, D., Rosen, M. K., & Schreiber, S. L. (1993) *J. Am. Chem. Soc. 115*, 819−820.

BI960975P